Mice Make Targeted Saccades

Sebastian H. Zahler[1,2,4], David E. Taylor[1,2,4], Julia M. Adams[1], and Evan H. Feinberg[1,2,3,*]

1. Department of Anatomy, University of California, San Francisco, San Francisco, CA 94158
2. Neuroscience Graduate Program, University of California, San Francisco, San Francisco, CA 94158
3. Kavli Institute for Fundamental Neuroscience, University of California, San Francisco, San Francisco, CA 94158
4. These authors contributed equally
*Corresponding author: evan.feinberg@ucsf.edu

Abstract:

Humans read text, recognize faces, and process emotions using targeted saccadic eye movements. In the textbook model, this innate ability to make targeted saccades evolved in species with foveae or similar high-acuity retinal specializations that enable scrutiny of salient stimuli. According to the model, saccades made by species without retinal specializations (such as mice) are never targeted and serve only to reset the eyes after gaze-stabilizing movements. Here we show that mice innately make touch-evoked targeted saccades. Optogenetic manipulations revealed the neural circuit mechanisms underlying targeted saccades are conserved. Saccade probability is a U-shaped function of current eye position relative to the target, mirroring the simulated relationship between an object's location within the visual field and the probability its next movement carries it out of view. Thus, a cardinal sophistication of our visual system may have had an unexpectedly early origin as an innate behavior that keeps stimuli in view.

Introduction:

Saccades, our most frequent movement, profoundly shape our lives. Humans and other vertebrates with foveae or similar high-acuity retinal specializations (e.g., areas centralis) innately make targeted saccades towards salient stimuli, whether text on a page, the sound of prey in the brush, or a tap on the hand (Kandel et al., 2013; Land, 2019; Land and Nilsson,

2012; Liversedge et al., 2011; Walls, 1962). In contrast, species with more uniform retinae (including rodents) have never been observed exhibiting this innate behavior despite their reliance on vision to execute a diverse array of appetitive, avoidance, discrimination, and attentional behaviors (Burgess et al., 2017; Hoy et al., 2016; Huberman and Niell, 2011; Land, 2019; Land and Nilsson, 2012; Meyer et al., 2018, 2020; Michaiel et al., 2020; Wallace et al., 2013; Yilmaz and Meister, 2013). These observations have led to the prevailing view that targeted saccades are sophisticated movements that evolved in species able to exploit high-acuity retinal specializations for scrutiny of salient stimuli, whereas saccades made by mammals with more uniform retinae are merely compensatory, functioning to re-center the eyes within the orbits following image-stabilizing eye movements that occur during head and body rotations (Kandel et al., 2013; Land, 2019; Land and Nilsson, 2012; Liversedge et al., 2011; Walls, 1962).

The absence of evidence of innate targeted saccades in mammals with more uniform retinae is puzzling, however, because neuroanatomical and functional studies suggest that the circuits that underlie sensory-evoked targeted saccades are conserved (May, 2005; Sparks, 1986, 2002). Specifically, the superior colliculus (SC) in mice contains a topographic map of saccade direction and amplitude (Wang et al., 2015) roughly aligned with maps of visual, auditory, and somatosensory space (Drager and Hubel, 1975, 1976). These SC sensory and motor maps closely resemble those believed to underlie primates' and cats' ability to make targeted saccades towards stimuli of these modalities (Sparks, 1986, 2002). We therefore hypothesized that targeted saccades are an ancient innate behavior that predates foveae, with afoveate mammals (i.e., those whose retinae lack high-acuity specializations) possessing a conserved, innate ability to generate targeted saccadic gaze shifts that had been overlooked.

Results:

To test the hypothesis that afoveate mammals possess a conserved ability to make targeted saccades, we head-fixed naïve, wild-type adult mice and used an infrared camera to track their left pupils. Previous studies examining the effects of visual stimuli on eye movements in freely moving and head-fixed rodents did not find evidence of saccade targeting (Meyer et al., 2018, 2020; Michaiel et al., 2020; Samonds et al., 2018; Wallace et al., 2013). We therefore asked whether mice make targeted saccades towards stimuli of other modalities. We used a multisensory stimulus consisting of airpuffs that deflected the whiskers and generated a loud, broadband sound. We delivered these loud airpuffs to the whiskers on either side every 7-12 s in a pseudorandom sequence (Fig. 1A). The probability of horizontal eye movements increased sharply 20-150 ms after stimulus presentation (Fig. 1B, Supplementary Fig. 1). These movements were saccade-like in that they reached velocities of several hundred degrees per second (Supplementary Fig. 2), displayed a main sequence, i.e., peak velocity scaled linearly with amplitude (Supplementary Fig. 2), and were bilaterally conjugate (Supplementary Fig. 3). We term this behavior the whisker-induced saccade-like reflex (WISLR).

If WISLR saccades are targeted, their endpoints should be largely independent of initial eye position but strongly dependent on the site of sensory stimulation. To determine whether endpoints were independent of initial eye position, we binned saccades according to initial eye position and examined average saccade trajectories and endpoints from each bin. Strikingly, average saccade trajectories converged on nearly the same endpoint regardless of starting eye position (Fig. 1C-E). Convergence of saccades on a common endpoint arose because saccade direction and amplitude varied systematically as a function of initial eye position (Fig. 1F-H). To determine whether saccade endpoints depended on the site of sensory stimulation, we compared saccades evoked by stimulation of the right and left whiskers. We observed that average trajectories varied with stimulus location such that the endpoint for saccades evoked by

stimulation of the left whiskers was to the left of the endpoint for saccades evoked by stimulation of the right whiskers (Fig. 1C-E). To further test whether the site of stimulation specified saccade targeting, we repositioned the airpuff nozzle to stimulate the ears, which are peripheral to the whiskers. As with the whisker stimuli, airpuffs applied to the ears evoked targeted saccades, and the endpoints were peripheral to those evoked by airpuff stimulation of the whiskers (left whiskers vs. left ear, $P = 0.0046$; right whiskers vs. right ear, $P = 0.0074$, paired two-tailed Student's t-test) (Fig. 2A, B, F). In addition, unlike the compensatory re-centering saccades previously observed in mice, saccades evoked by ear airpuffs were not centripetally directed and in fact were centrifugal from central eye positions (Fig. 2B). Therefore, we concluded that WISLR saccades are targeted.

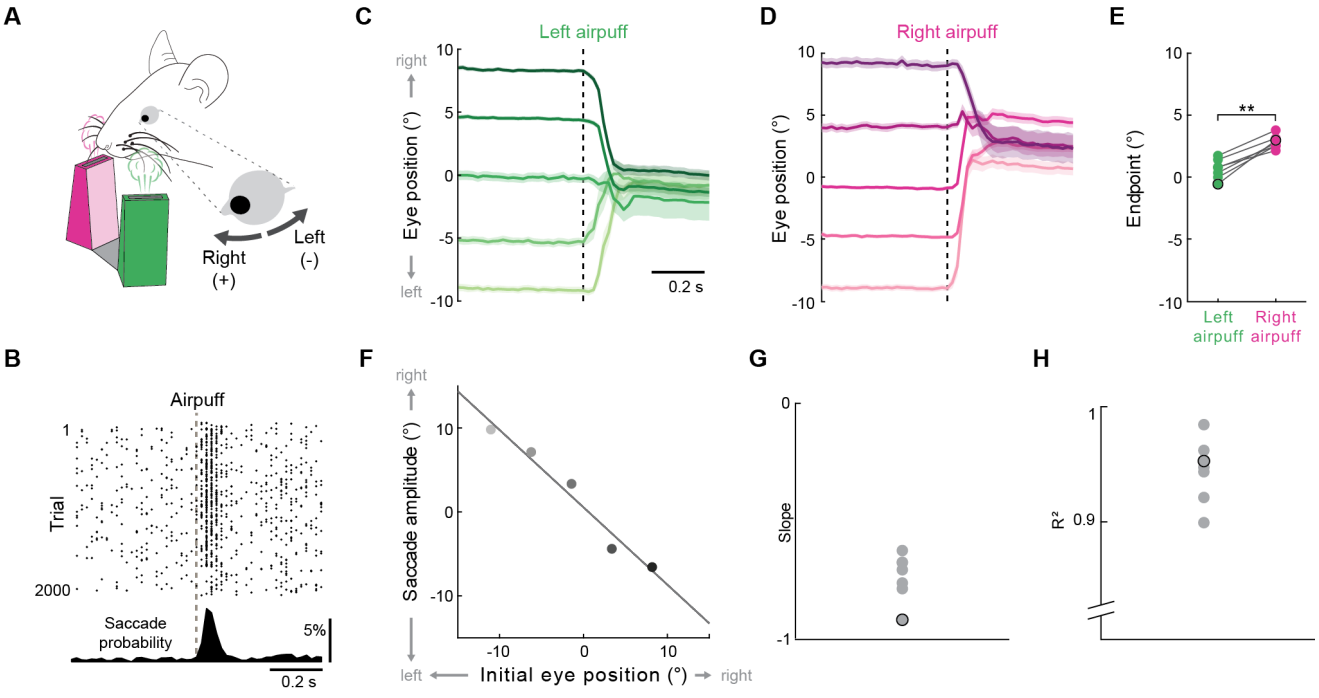

Figure 1. Mice innately make targeted saccades. (A) Behavioral setup schematic. Mice are head-fixed with airpuff nozzles positioned beneath the right and left whiskers. Airpuffs are presented on only one side per trial. Left eye position is tracked using a camera. In subsequent quantification, eye positions to the right of center (nasal) are positive, and eye positions to the left of center (temporal) are negative. **(B)** Top, saccade raster for six consecutive sessions for a representative mouse. Dashed line denotes airpuff onset, dots denote onset times of individual saccades. Bottom, peri-stimulus time histogram. **(C, D)** Mean saccade trajectories in response to airpuffs delivered to the left (C) or right (D) whiskers. Traces denote mean trajectories +/- s.e.m. from five different initial eye position bins for a representative mouse. 0° corresponds to the median eye position. Saccades occasionally undershot the endpoint by an amount that scaled with initial distance from the endpoint. Similar undershoots observed when other species are head-fixed are thought to occur because targeted gaze shifts ordinarily comprise eye and head movements yet the latter are precluded by a head-fixed preparation (Liversedge et al., 2011). Consistent with this idea, measurements using load cells (also known as strain gauges) showed that WISLR saccades were accompanied by attempted head movements that scaled with saccade amplitude (Supplementary Fig. 4) (Meyer et al., 2020). **(E)** Mean saccade endpoints for individual mice (n = 7 mice) in response to left and right whisker stimulation (**P <0.001, paired two-tailed Student's t-test). Black outlines indicate values for the example mouse in (C, D). **(F)** Relationship between airpuff-evoked saccade amplitude and initial eye position for the example mouse in (C, D). **(G, H)** Slope of relationship between eye position and saccade amplitude (G) and coefficient of determination (H) for individual mice (n = 7 mice) in response to left and right whisker stimulation. Black outlines indicate values for mouse in (C, D).

Because the WISLR airpuff stimulus provides both auditory and tactile inputs, it was unclear whether targeted saccades required multisensory synergy. To uncouple auditory and tactile contributions, we first moved the airpuff nozzles 5 cm away from the mouse while maintaining the same azimuthal position such that the airpuff could provide auditory but not tactile stimulation (Fig. 2C). We then presented airpuffs on either the right or the left side of the mouse in a pseudorandom sequence. As in the WISLR, these auditory-only airpuffs evoked saccades

(Supplementary Fig. 5). However, the endpoint locations did not differ for left and right auditory stimuli (Fig. 2C, F, G). We compared the sound-evoked saccade endpoint location to that of centripetally directed spontaneous saccades and found no significant difference (Fig. 2E-G) (Land and Nilsson, 2012; Meyer et al., 2018, 2020; Michaiel et al., 2020; Paré and Munoz, 2001; Tatler, 2007). The convergence of both auditory and spontaneous saccades on a common central location suggests that auditory stimuli are sufficient to increase the probability of centripetal saccade generation but do not provide targeting information.

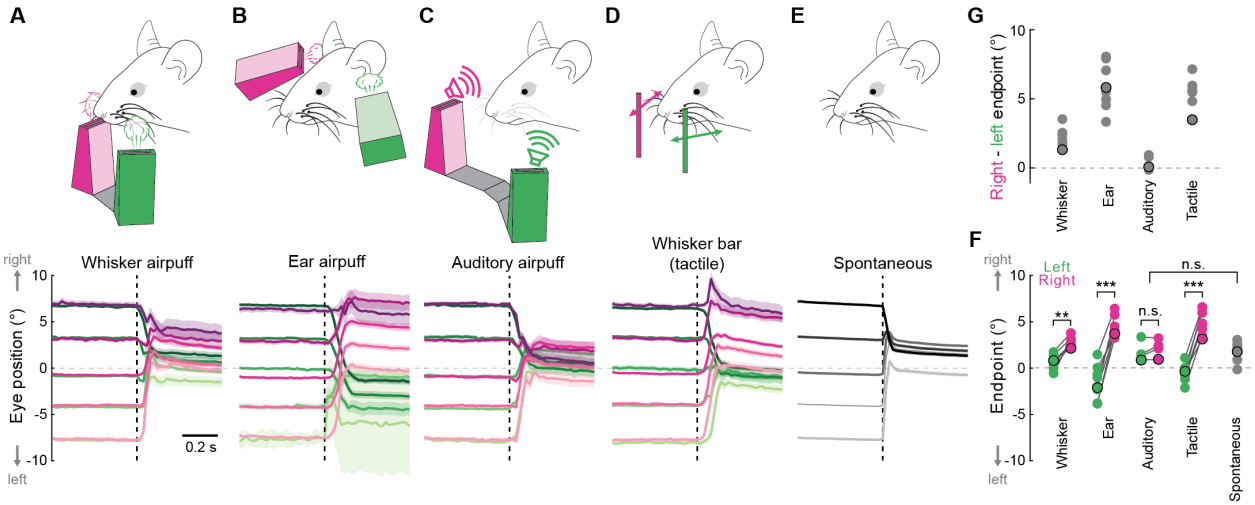

Figure 2. Tactile but not auditory stimulation specifies saccade endpoint. (A-D) Schematic of behavioral setup (top) and mean saccade trajectories (bottom) for left (green traces) or right (magenta traces) whisker airpuff (A), ear airpuff (B), auditory (C), and whisker bar (D) stimuli. Dashed lines denote stimulus onset. **(E)** Mean trajectories for spontaneous saccades. Traces denote mean trajectories +/- s.e.m. from five different initial eye position bins for a representative mouse. **(F, G)** Mean endpoints (F) and difference in mean endpoints (G) for saccades evoked by left or right stimuli for individual mice (whisker airpuff, n = 7 mice; ear airpuff, n = 8 mice; whisker bar, n = 8 mice; auditory, n = 4 mice; spontaneous, n = 8 mice) (n.s., not significant ; $^{**}P < 0.001$; $^{***}P < 0.0001$, paired two-tailed Student's t-test). Black outlines indicate values for mouse in (A-E).

To determine whether tactile input was sufficient to evoke targeted saccades, we used a metal bar to nearly silently deflect the whiskers on either side of the mouse in a pseudorandom sequence (Fig. 2D). Interestingly, the endpoints of saccades evoked by the bar stimulus differed for the left and right whiskers, indicating that tactile stimulation, unlike auditory stimulation, is sufficient to specify the saccade target (Fig. 2D, F, G). Thus, both the auditory and tactile

components of the airpuff stimuli are sufficient to evoke saccades but only tactile stimulation evokes targeted saccades whose endpoints are specified by the site of stimulation.

These behavioral findings revealed that mice are capable of targeted saccades that closely resemble those made by foveates. This behavioral similarity could reflect a common origin in an ancestral species or convergent evolution. We reasoned that if the former is the case, the neural control mechanisms should be the same for targeted saccades across species. In contrast, if the neural control mechanisms differed between mice and other species, we would conclude that targeted saccades arose independently in these species. In primates and cats, SC serves as a command center for the control of targeted saccades (Sparks, 1986, 2002). To determine whether SC control of saccade targeting is conserved in the WISLR, we used optogenetics to manipulate right SC activity in the period surrounding airpuff onset. For inhibition experiments, we stereotaxically injected adeno-associated virus (AAV) encoding the light-gated chloride pump eNpHR3.0 under the control of a pan-neuronal promoter and implanted a fiber optic in right SC (Fig. 3A). Consistent with data in foveate species (Hikosaka and Wurtz, 1985; Robinson, 1972; Schiller and Stryker, 1972), optically reducing right SC activity shifted airpuff-evoked saccade endpoints to the right (i.e., ipsilaterally), whereas illumination in control animals expressing a fluorophore in SC caused no effect on saccades (Fig. 3B-D, Supplementary Fig. 6). For stimulation experiments, we stereotaxically injected AAV encoding the light-gated ion channel ChR2 under the control of a pan-neuronal promoter and implanted a fiber optic in right SC (Fig. 3E). Because strong SC stimulation can evoke saccades, we used weak, subthreshold stimulation (10 μW) in order to bias SC activity without optogenetically triggering saccades. These subthreshold increases of right SC activity shifted airpuff-evoked saccade endpoints to the left (i.e., contralaterally) (Fig. 3F-H). Therefore, we concluded that SC underlies the generation of targeted saccades in the WISLR, indicating that the neural circuitry and computations are conserved across species.

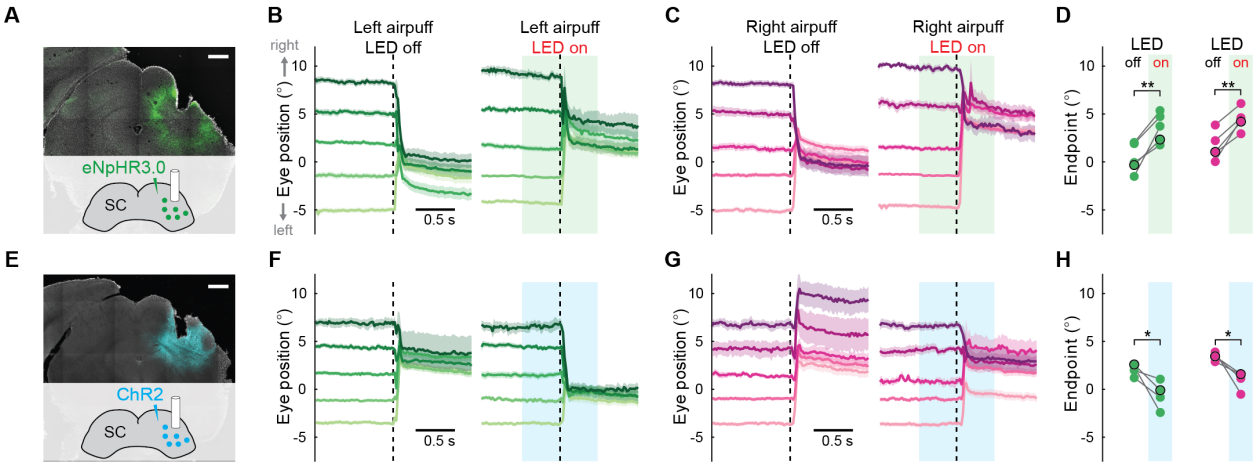

Figure 3. **Superior colliculus controls mouse targeted saccades. (A)** Schematic of right SC optogenetic inhibition and example histology for representative mouse shown in (B-D). Scale bar, 0.5 mm. The lack of fluorescence immediately surrounding fiber tip is due to photobleaching by high photostimulation intensity (6 mW, as opposed to 10 μW for ChR2 experiments in (E-H). **(B)** Mean saccade trajectories in response to airpuffs delivered to left whiskers on control (left) and optogenetic inhibition (right) trials for a representative mouse. Traces denote mean trajectories +/- s.e.m. from five different initial eye position bins. Dashed line denotes airpuff onset. Green shading denotes period of LED illumination. **(C)** As in (B) for airpuffs delivered to right whiskers. **(D)** Mean endpoints for saccades evoked by left (left) or right (right) whisker airpuffs on control (white background) and SC optogenetic inhibition (green background) trials for individual mice (n = 5) (**P < 0.001, paired two-tailed Student's t-test). **(E)** Schematic of right SC subthreshold optogenetic stimulation and example histology for mouse shown in (F-H). **(F)** Mean saccade trajectories in response to airpuffs delivered to left whiskers on control (left) and subthreshold optogenetic stimulation (right) trials for a representative mouse. Traces denote mean trajectories +/- s.e.m. from five different initial eye-position bins. Dashed line denotes airpuff onset. Blue shading denotes period of LED illumination. Note that this weak, subthreshold stimulation (10 μW) does not evoke saccades at LED onset, as is observed at higher light intensities. **(G)** As in (F) for airpuffs delivered to right whiskers. **(H)** Right, mean endpoints for saccades evoked by left or right whisker airpuffs on control (white background) and SC optogenetic stimulation (blue background) trials for individual mice (n = 4) (*P < 0.05, paired two-tailed Student's t-test).

These findings suggested that targeted saccades in response to salient stimuli are an ancient innate behavior that evolved in mammals prior to specializations such as the fovea. We sought to identify why it would have been adaptive for an ancestral species to ensure that a stimulus is imaged on a particular region of a uniform retina. Because the WISLR is probabilistic, we reasoned that we could infer potential functions by identifying factors that controlled saccade probability. We first examined arousal, which modulates many neuronal and behavioral phenomena. Surprisingly, saccade probability did not differ between trials with high (dilated pupils) or low (constricted pupils) arousal (Fig. 4A) (Reimer et al., 2014). Next, we asked whether novelty played a role by examining the effects of sensory history. Saccade probability was constant both within and across sessions, suggesting that these responses did not potentiate or habituate (Fig. 4B, C). We then examined eye position. Strikingly, saccade

probability was a U-shaped function of initial eye position, with higher probabilities at more eccentric eye positions (Fig. 4D). These U-shaped functions were offset for left and right whisker airpuffs (Fig. 4D), with the trough of each curve coinciding with the endpoint of saccades evoked by each stimulus (Fig. 4E). We considered why it would be adaptive for mice to be more likely to saccade the further their current eye position is from the endpoint. We intuited that the closer a stimulus is to the edge of the visual field, the higher the likelihood that its next movement will carry it out of the field of view and thus the greater the impetus to make a saccade (Fig. 4F). We therefore hypothesized that targeted saccades keep salient stimuli in view, with the U-shaped relationship between eye position and saccade probability a result of the underlying relationship between stimulus location and the likelihood the stimulus will leave the visual field. To test this hypothesis, we performed simulations to determine the relationship between stimulus location and the probability its next movement carries it out of view. Because the whisker stimuli we used are lateral, we performed modeling for monocular fields of view. Consistent with our prediction, for both Gaussian and uniform distributions of movement amplitudes and over a wide range of distribution widths, the probability of a stimulus leaving the visual field was a U-shaped function of its location, strikingly similar to the probability of a saccade as a function of distance from initial eye position to the endpoint (Fig. 4G, H). We thus concluded that our experimental and simulation data are consistent with a model in which targeted saccades would help to keep stimuli within the field of view. In this way, targeted saccades would be adaptive even for a species with perfectly uniform retinae.

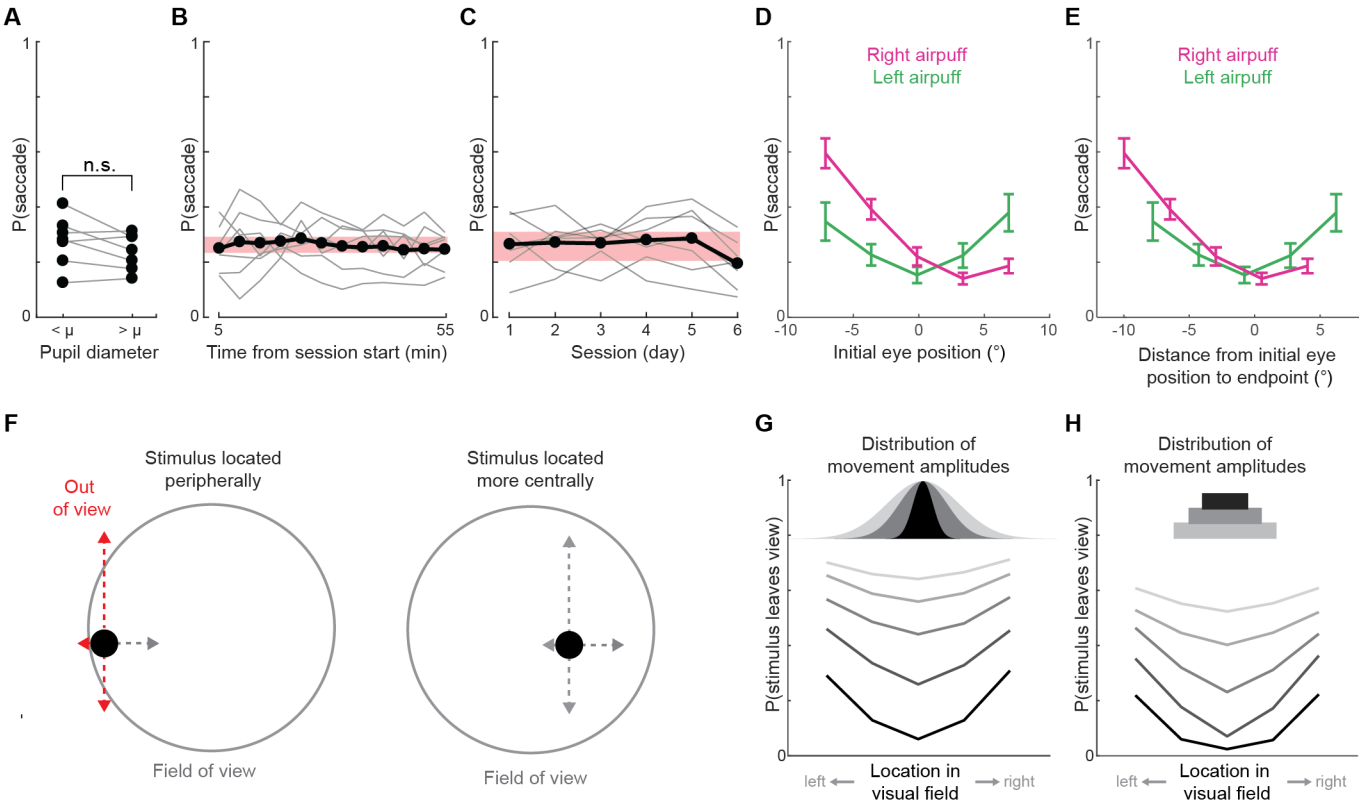

Figure 4. Targeted saccades keep salient stimuli in view. (A). Probability of saccades on trials with high (pupil diameter greater than the mean, μ) and low (pupil diameter less than μ) arousal. Each black dot corresponds to an individual mouse (n = 7 mice) (n.s., not significant, paired two-tailed Student's t-test). **(B)** Saccade probability within sessions. Sessions were binned into five-minute intervals and mean probabilities within each were determined. Thin gray lines denote individual mice and black lines denote population mean. Red shading denotes bootstrapped 99% confidence interval of the mean for the session. **(C)** Saccade probability across sessions. Red shading denotes bootstrapped 99% confidence interval of the mean across days. **(D)** Relationship between eye position and saccade probability. Green and magenta lines indicate population means (n = 7 mice) for left and right airpuffs, respectively. Error bars indicate s.e.m. **(E)** Relationship between distance from initial eye position to target and saccade probability. **(F)** Model. In this schematic, an example stimulus (black circle) starts at two locations in the visual field, one in the periphery and one more central. Potential movements (arrows) can be made in any direction and over a range of amplitudes but only cardinal directions are illustrated. Gray arrows denote movements that would not carry the stimulus out of the field of view, red arrows denote movements that would carry the stimulus out of the field of view. **(G, H)** Relationships between stimulus location in visual field and probability that the stimulus' next movement carries it out of view for normally (G) and uniformly (H) distributed movement amplitudes. Different line shadings correspond to simulations using narrower (black) or wider (gray) distribution widths (see methods) (n = 100,000 simulations for each).

Discussion:

We have shown that mice innately make saccadic eye movements towards tactile stimuli. Previous studies in head-fixed mice observed occasional undirected saccades in response to changes in the visual environment (Samonds et al., 2018) and visually guided saccades could be elicited only after weeks of training and at extremely long (~1 s) latencies (Itokazu et al., 2018). Similarly, studies in freely moving rodents have found no evidence of saccade targeting,

suggesting instead that rodents use saccades to move the eyes centripetally following gaze-stabilizing eye movements made during head and body movements, as is reported in other afoveates (Meyer et al., 2018, 2020; Michaiel et al., 2020; Wallace et al., 2013). We observed that mice attempted to make similar head movements to accompany WISLR saccades; it will be interesting in future studies to investigate WISLR head-eye coupling in freely moving mice. Intriguingly, both auditory and tactile stimuli were sufficient to evoke saccades, but only tactile stimuli evoked targeted saccades. Whether this is due to differences in the spatial acuities of these sensory systems, the salience of tactile and auditory stimuli in general, or features of the specific stimuli we used will be of interest to investigate in the future. More broadly, our findings suggest that analyzing eye movements of other afoveate species thought not to make targeted saccades—such as rabbits, toads, and goldfish—in response to a broad range of multimodal stimuli may uncover similar abilities.

We also found that the circuit mechanisms underlying targeted saccades in carnivores and primates are conserved in rodents (May, 2005; Sparks, 1986, 2002). One practical implication of this finding is that the WISLR could be applied to the study of several outstanding questions. First, there are many unresolved problems regarding the circuitry and ensemble dynamics underlying target selection (Basso and May, 2017) and saccade generation (Gandhi and Katnani, 2011), and the mouse provides a genetically tractable platform with which to investigate these and other topics. Second, gaze shifts are aberrant in a host of conditions, such as Parkinson's and autism spectrum disorder (Liversedge et al., 2011). We expect that the WISLR paradigm will be a powerful tool for the study of mouse models of a variety of neuropsychiatric conditions. Third, targeting gaze shifts requires an ability to account for the initial positions of the eyes relative to the target, a phenomenon also known as remapping from sensory to motor reference frames. Neural correlates of this process have been observed in primates (Groh and Sparks, 1996; Jay and Sparks, 1984) and cats (Populin et al., 2004), but the

underlying circuitry and computations remain obscure. The WISLR may facilitate future studies of this problem. Thus, the WISLR behavior is likely to be a powerful tool for myriad lines of investigation.

The extensive conservation from mice to primates of both behavior and neuroanatomy argues that targeted saccades evolved much earlier than previously thought. Prior to our study, it was believed that species with high-acuity retinal specializations acquired the ability to make targeted saccades to scrutinize salient environmental stimuli, because animals lacking such retinal specializations were thought incapable of targeted saccades (Land, 2019; Land and Nilsson, 2012; Liversedge et al., 2011; Walls, 1962). The discovery that targeted saccades are phylogenetically ancient raises the question of what fovea-independent functions these movements initially served. In attempting to understand why targeted saccades would be adaptive for such species, we observed that saccade probability was a U-shaped function of the distance from initial eye position to the endpoint. We reasoned that the stronger drive to saccade from eye positions further from the endpoint may reflect an increased probability that a salient stimulus moves out of view the closer it is to the edge of the visual field. To test this hypothesis, we performed simulations that revealed a strikingly similar U-shaped relationship between stimulus location in the visual field and the probability its next movement carries it out of view. Thus, even if a species had perfectly uniform retinae, a targeted saccade that changes where on the retina a stimulus projects would facilitate keeping it in view.

Nevertheless, it is worth noting that mice do not have perfectly uniform retinae. Although mouse retinae lack discrete, anatomically defined specializations such as foveae or areas centralis, there are subtler nonuniformities in the distribution and density of photoreceptors and retinal ganglion cell subtypes, and magnification factor, receptive field sizes, and response tuning vary across the visual field in higher visual centers (Ahmadlou and Heimel, 2015; Baden et al., 2013;

Bleckert et al., 2014; Drager and Hubel, 1976; Feinberg and Meister, 2015; Li et al., 2020; de Malmazet et al., 2018). It is possible that saccadic eye movements ensure that salient stimuli fall into a partially specialized region of the visual field; this would also be associated with a U-shaped drive to make saccades as a function of eye position relative to the desired endpoint. Finally, because tactile stimuli typically derive from proximal objects and as a result may require rapid responses, the speed of saccades relative to head movements may be especially beneficial.

In conclusion, we have revealed that the targeted saccade is an innate behavior that is not exclusive to species with highly sophisticated retinae. Prior studies in diverse species whose retinae lack high-acuity specializations had never observed targeted saccades, but by testing stimuli different from those previously examined we revealed that mice make targeted saccades. Detailed perturbation experiments determined that the circuit mechanisms of sensory-evoked targeted saccades are conserved from mice to humans, suggesting that this behavior arose in a common, afoveate ancestral species long ago. Finally, mathematical modeling identified how targeted saccades would have been adaptive for such an ancestral species even if it had perfectly uniform retinae. Taken together, our findings reveal that an ostensible hallmark of humans and other highly visual species is an ancient innate behavior used to hold salient stimuli in view.

Acknowledgments: We thank M. Brainard, J. Horton, A. Krishnaswamy, M. Scanziani, and members of the Feinberg laboratory for helpful discussions and comments on the manuscript. This work was supported by departmental funds and grants from the E. M. Ziegler Foundation for the Blind, Sandler Foundation, Klingenstein-Simons Fellowship Award in Neuroscience, Brain and Behavior Research Foundation (NARSAD Young Investigator Awards 25337 and 27320), Whitehall Foundation, Simons Foundation (SFARI 574347), and US National Institutes

of Health (DP2 MH119426 and R01 NS109060) to E.H.F.

Author contributions: S.H.Z., D.E.T., and E.H.F. conceived of the project, designed the experiments, analyzed the data, and prepared the manuscript. S.H.Z. and D.E.T. discovered and characterized the WISLR behavior. S.H.Z. and J.M.A. conducted the optogenetic experiments. E.H.F. performed the simulations.

Competing interests: The authors declare no competing interests.

References:

Ahmadlou, M., and Heimel, J.A. (2015). Preference for concentric orientations in the mouse superior colliculus. Nat. Commun. *6*.

Baden, T., Schubert, T., Chang, L., Wei, T., Zaichuk, M., Wissinger, B., and Euler, T. (2013). A tale of two retinal domains: Near-Optimal sampling of achromatic contrasts in natural scenes through asymmetric photoreceptor distribution. Neuron *80*, 1206–1217.

Basso, M.A., and May, P.J. (2017). Circuits for Action and Cognition: A View from the Superior Colliculus. Annu. Rev. Vis. Sci. *3*, 197–226.

Bleckert, A., Schwartz, G.W., Turner, M.H., Rieke, F., and Wong, R.O.L. (2014). Visual space is represented by nonmatching topographies of distinct mouse retinal ganglion cell types. Curr. Biol. *24*, 310–315.

Burgess, C.P., Lak, A., Steinmetz, N.A., Zatka-Haas, P., Bai Reddy, C., Jacobs, E.A.K., Linden, J.F., Paton, J.J., Ranson, A., Schröder, S., et al. (2017). High-Yield Methods for Accurate Two-Alternative Visual Psychophysics in Head-Fixed Mice. Cell Rep. *20*, 2513–2524.

Drager, U.C., and Hubel, D.H. (1975). Responses to visual stimulation and relationship between visual, auditory, and somatosensory inputs in mouse superior colliculus. J. Neurophysiol. *38*, 690–713.

Drager, U.C., and Hubel, D.H. (1976). Topography of visual and somatosensory projections to mouse superior colliculus. J. Neurophysiol. *39*, 91-101.

Feinberg, E.H., and Meister, M. (2015). Orientation columns in the mouse superior colliculus. Nature *519*, 229–232.

Gandhi, N.J., and Katnani, H.A. (2011). Motor Functions of the Superior Colliculus. Annu. Rev. Neurosci. *34*, 205–231.

Groh, J.M., and Sparks, D.L. (1996). Saccades to somatosensory targets. III. Eye-position-dependent somatosensory activity in primate superior colliculus. J. Neurophysiol. *75*, 439–453.

Hikosaka, O., and Wurtz, R.H. (1985). Modification of saccadic eye movements by GABA-related substances. I. Effect of muscimol and bicuculline in monkey superior colliculus. J. Neurophysiol. *53*, 266–291.

Hoy, J.L., Yavorska, I., Wehr, M., and Niell, C.M. (2016). Vision Drives Accurate Approach Behavior during Prey Capture in Laboratory Mice. Curr. Biol. *26*, 3046–3052.

Huberman, A.D., and Niell, C.M. (2011). What can mice tell us about how vision works? Trends Neurosci. *34*, 464–473.

Itokazu, T., Hasegawa, M., Kimura, R., Osaki, H., Albrecht, U.R., Sohya, K., Chakrabarti, S., Itoh, H., Ito, T., Sato, T.K., et al. (2018). Streamlined sensory motor communication through cortical reciprocal connectivity in a visually guided eye movement task. Nat. Commun. *9*.

Jay, M.F., and Sparks, D.L. (1984). Auditory receptive fields in primate superior colliculus shift with changes in eye position. Nature *309*, 345–347.

Kandel, E.R., Schwartz, J.H., Jessell, T.M., Siegelbaum, S.A., and Hudspeth, A.J. (2013). Principles of Neural Science, Fifth Editon | Neurology Collection | McGraw-Hill Medical.

Land, M.F. (2019). The Evolution of Gaze Shifting Eye Movements. Curr. Top. Behav. Neurosci. *41*, 3–11.

Land, M.F., and Nilsson, D.-E. (2012). Animal Eyes.

Li, Y. tang, Turan, Z., and Meister, M. (2020). Functional Architecture of Motion Direction in the Mouse Superior Colliculus. Curr. Biol. *30*, 3304–3315.

Liversedge, S.P., Gilchrist, I.D., and Everling, S. (2011). The Oxford Handbook of Eye Movements (Oxford: Oxford Univerity Press).

de Malmazet, D., Kühn, N.K., and Farrow, K. (2018). Retinotopic Separation of Nasal and Temporal Motion Selectivity in the Mouse Superior Colliculus. Curr. Biol. *28*, 2961-2969.e4.

Mathis, A., Mamidanna, P., Cury, K.M., Abe, T., Murthy, V.N., Mathis, M.W., and Bethge, M. (2018). DeepLabCut: markerless pose estimation of user-defined body parts with deep learning. Nat. Neurosci. *21*, 1281–1289.

May, P.J. (2005). The mammalian superior colliculus: Laminar structure and connections. Prog. Brain Res. *151*, 321–378.

Meyer, A.F., Poort, J., OKeefe, J., Sahani, M., and Linden, J.F. (2018). A Head-Mounted Camera System Integrates Detailed Behavioral Monitoring with Multichannel Electrophysiology in Freely Moving Mice.

Meyer, A.F., O'Keefe, J., and Poort, J. (2020). Two Distinct Types of Eye-Head Coupling in Freely Moving Mice. Curr. Biol. *30*, 2116-2130.e6.

Michaiel, A.M., Abe, E.T., and Niell, C.M. (2020). Dynamics of gaze control during prey capture in freely moving mice. Elife *9*.

Paré, M., and Munoz, D.P. (2001). Expression of a re-centering bias in saccade regulation by superior colliculus neurons. Exp. Brain Res. *137*, 354–368.

Populin, L.C., Tollin, D.J., and Yin, T.C.T. (2004). Effect of eye position on saccades and neuronal responses to acoustic stimuli in the superior colliculus of the behaving cat. J. Neurophysiol. *92*, 2151–2167.

Reimer, J., Froudarakis, E., Cadwell, C.R., Yatsenko, D., Denfield, G.H., and Tolias, A.S. (2014). Pupil Fluctuations Track Fast Switching of Cortical States during Quiet Wakefulness. Neuron *84*, 355–362.

Robinson, D.A. (1972). Eye movements evoked by collicular stimulation in the alert monkey. Vision Res. *12*, 1795–1808.

Samonds, J.M., Geisler, W.S., and Priebe, N.J. (2018). Natural image and receptive field statistics predict saccade sizes. Nat. Neurosci. *21*, 1591–1599.

Schiller, P.H., and Stryker, M. (1972). Single-unit recording and stimulation in superior colliculus of the alert rhesus monkey. J. Neurophysiol. *35*, 915–924.

Sparks, D.L. (1986). Translation of sensory signals into commands for control of saccadic eye movements: role of primate superior colliculus. Physiol Rev. *66*, 118–171.

Sparks, D.L. (2002). The brainstem control of saccadic eye movements. Nat. Rev. Neurosci. *3*,

952–964.

Stahl, J.S., Van Alphen, A.M., and De Zeeuw, C.I. (2000). A comparison of video and magnetic search coil recordings of mouse eye movements. J. Neurosci. Methods *99*, 101–110.

Tatler, B.W. (2007). The central fixation bias in scene viewing: Selecting an optimal viewing position independently of motor biases and image feature distributions. J. Vis. *7*, 4.

Wallace, D.J., Greenberg, D.S., Sawinski, J., Rulla, S., Notaro, G., and Kerr, J.N.D. (2013). Rats maintain an overhead binocular field at the expense of constant fusion. Nature *498*, 65–69.

Walls, G.L. (1962). The evolutionary history of eye movements. Vision Res. *2*, 69–80.

Wang, L., Liu, M., Segraves, M.A., and Cang, J. (2015). Visual experience is required for the development of eye movement maps in the mouse superior colliculus. J. Neurosci. *35*, 12281–12286.

Yilmaz, M., and Meister, M. (2013). Rapid innate defensive responses of mice to looming visual stimuli. Curr. Biol. *23*, 2011–2015.

Materials and Methods

Mice: All experiments were performed according to Institutional Animal Care and Use Committee standard procedures. C57BL/6J wild-type (Jackson Laboratory, stock 000664) mice between 2 and 12 months of age were used. Mice were housed in a vivarium with a reversed 12:12 h light:dark cycle and tested during the dark phase. No statistical methods were used to predetermine sample size. Behavioral experiments were not performed blinded as the experimental setup and analyses are automated.

Surgical procedures: Mice were administered carprofen (5 mg/kg) 30 minutes prior to surgery. Anesthesia was induced with inhalation of 2.5% isoflurane and buprenorphine (1.5 mg/kg) was administered at the onset of the procedure. Isoflurane (0.5-2.5% in oxygen, 1 L/min) was used to maintain anesthesia and adjusted based on the mouse's breath and reflexes. For all surgical procedures, the skin was removed from the top of the head and a custom titanium headplate was cemented to the leveled skull (Metabond, Parkell) and further secured with dental cement (Ortho-Jet powder, Lang Dental). Craniotomies were made using a 0.5 mm burr and viral vectors were delivered using pulled glass pipettes coupled to a microsyringe pump (Micro4, World Precision Instruments) on a stereotaxic frame (Model 940, Kopf Instruments). Following surgery, mice were allowed to recover in their home cages for at least 1 week.

Viral injections and implants: Coordinates for SC injections were ML: 1.25 mm, AP: 0.7 mm (relative to lambda), DV: -1.9 and -2.1 mm (100 nL/depth). Coordinates for SC implants were ML: 1.25 mm, AP: 0.7 mm (relative to lambda), DV: -2.0 mm. Fiber optic cannulae were constructed from ceramic ferrules (CFLC440-10, Thorlabs) and optical fiber (400 mm core, 0.39 NA, FT400UMT) using low-autofluorescence epoxy (F112, Eccobond).

Behavioral procedures: During experiments, headplated mice were secured in a custom 3D-printed mouse holder. Timing and synchronization of the behavior were controlled by a

microcontroller (Arduino MEGA 2560 Rev3, Arduino) receiving serial commands from custom Matlab scripts. All experiments were performed using awake mice. To maintain a clear line of sight between pupil and camera, whiskers A1, A2, B1, and B2 were trimmed 1 day prior to the first day of behavior and every 4-5 days subsequently. Left and right stimuli were randomly selected and presented at intervals drawn from a 7-12 s uniform distribution. Each session consisted of 360 stimulus presentations and lasted ~60 minutes. No training or habituation was necessary.

WISLR characterization: All data for figures 1 and 2 were collected from 8 mice over 28 days (1 session/mouse/day). Session types were randomly interleaved to yield a total of 8 whisker airpuff sessions, 6 ear airpuff sessions, 8 auditory sessions, and 6 whisker bar sessions.

Stimuli: Airpuff stimuli were generated using custom 3D-printed airpuff nozzles (1.5 mm wide, 10 mm long) connected to compressed air that was gated by a solenoid. 3D-printed nozzles were used to standardize stimulus alignment across experimental setups but similar results were obtained in preliminary experiments using a diverse array of nozzle designs. For whisker airpuffs, the nozzles were spaced 24 mm apart and centered 10 mm beneath the mouse's left and right whiskers.For ear airpuffs, the nozzles were directed toward the ears while maintaining 10 mm of separation between the nozzles and the mouse. For auditory-only airpuffs, the nozzles were moved 50 mm away from the mouse while maintaining the same azimuthal position. For tactile-only stimulation, the whiskers were deflected along an axis parallel to whisking motion and ~10 mm away from the mouse's face using an L-key (7122A37, McMaster) attached to a stepper motor (1568-1105-ND, DigiKey). The stepper motor was sandwiched between rubber pads (8514K61, McMaster) and elevated on rubber pedestals (20125K73, McMaster) to reduce sound due to vibration.

Eye tracking: In most experiments, the movement of the left eye was monitored at 50 Hz using a high-speed camera (Fl3-U3-13Y3M-C1/2", Flir) coupled to a 110 mm working distance 0.5X telecentric lens (#67- 303, Edmund Optics). In the subset of experiments that examined the relationship between saccade amplitude and velocity and bilateral eye movements, both eyes were recorded at 200 Hz. A bandpass filter (FB850-40, Thorlabs) was attached to the lens to block visible illumination. Three IR LEDs (475-1200-ND, DigiKey) were used to illuminate the eye and one was aligned to the camera's vertical axis to generate a corneal reflection. In a subset of experiments, attempted head movements were measured by inserting load cell force sensors (Sparkfun, SEN-14727) between the mouse's headplate and the head-fixation assembly. Videos were processed post hoc using DeepLabCut, a machine learning package for tracking pose with user-defined body parts (Mathis et al., 2018). Data in this paper were analyzed using a network trained on 1000 frames of recorded behavior from 8 mice (125 frames per mouse). The network was trained to detect the left and right edges of the pupil and the left and right edges of the corneal reflection. Frames with a DeepLabCut-calculated likelihood of $P < 0.99$ were discarded from analyses. Angular eye position (E) was determined using the formula:

$$E = \arcsin((CR - P)/R_p)$$

where CR is the position of the corneal reflection, P is the position of the pupil center, and R_p is the estimated radius of rotation of the pupil. An estimate of R_p (1.08 mm) was determined using the methods described in Stahl et al., 2000 (Stahl et al., 2000). Briefly, the camera was rotated ±10° around the pupil and the values of the CR-P difference taken at the two extremes of camera position were used to estimate R_p.

Optogenetics: Optogenetic experiments were performed using the whisker airpuff nozzles. Fiber optic cables were coupled to implanted fibers and the junction was shielded with black heat

shrink. A 470 nm fiber-coupled LED (M470F3, Thorlabs) was used to excite ChR2-expressing neurons, and a 545 nm fiber-coupled LED (UHP-T-SR, Prizmatix) was used to inhibit eNpHR3.0-expressing neurons. Optogenetic excitation during WISLR sessions was delivered on a random 50% of trials using 1 s of illumination centered around airpuff onset.

SC inhibition: For optogenetic inactivation of SC neurons, AAV1.hSyn.eNpHR3.0 was injected in right SC of 5 wild-type mice. Experiments were performed 36-42 days post injection. LED power was 6 mW. Mice underwent 5 sessions each.

SC stimulation: For subthreshold optogenetic stimulation of SC neurons, AAV1.CaMKIIa.hChR2(H134R)-EYFP was injected in right SC of 4 wild-type mice. Experiments were performed 10-14 days post injection. LED power was 10 μW. Mice underwent 3 sessions each.

SC control: To control for the effects of light and viral expression, AAV9.CaMKII.GCaMP6s was injected in SC of 4 wild-type mice. Experiments were performed 18-36 days post injection. LED power was 6 mW. Mice underwent 5 WISLR sessions each.

Histology: For histological confirmation of fiber placement and injection site, mice were perfused with PBS followed by 4% PFA. Brains were removed and post-fixed overnight in 4% PFA, and stored in 20% sucrose solution for at least 1 day. Brains were sectioned at 50 μm thickness using a cryostat (NX70, Cryostar), every third section was mounted, and slides were cover-slipped using DAPI mounting medium (Southern Biotech). Tile scans were acquired using a confocal microscope (LSM700, Zeiss) coupled to a 10X air objective.

Saccade detection: Saccades were defined as eye movements that exceeded 100°/s, were at least 2° in amplitude, and were not preceded by a saccade in the previous 100 ms. The initial positions and endpoints of saccades were defined as the first points at which saccade velocity

rose above or fell below 50°/s, respectively. Analyses focused on horizontal saccades because saccades were strongly confined to the azimuthal axis (Supplementary Fig. 1).

Behavioral analysis: Stimulus-evoked saccades were defined as those within 150 ms of stimulus onset. Mice were excluded for a given stimulus type (e.g., whisker airpuff) if the probability of a saccade during the response window across all sessions was below 5%.

To visualize saccade trajectories for left and right stimulus-evoked saccades for individual mice (as in Fig.1C, D, 2A-D, 3B, C, E, & F), data were binned by initial eye position and averaged. Only trials in which the mouse maintained fixation in the 500 ms preceding stimulus onset, generated a saccade in the 150 ms response window, and maintained fixation in the 350 ms following the response window were included. Evenly spaced bins were generated between outer bin boundaries set as the 5^{th} and 95^{th} percentiles of initial eye positions from which the mouse made stimulus-evoked saccades. In Fig. 1, bins were determined using pooled left and right whisker airpuff trials. In Fig. 2, bins were determined using pooled data for all stimulus types and directions. In Fig. 3, bins were determined using pooled LED-on and LED-off trials for left or right whisker airpuffs.

To plot initial eye position against saccade amplitude (Fig. 1F, G), left and right whisker airpuff trials were pooled and initial eye position values were adjusted to reflect distance from the mean endpoint for each trial type. The slope and R^2 values for each curve were determined using linear regression.

Simulations: To simulate the effects of stimulus location on the probability its next movement carries it out of the visual field, we modeled the visual field as a circle and started stimuli at locations whose distance from and angle with respect to the center were drawn from uniform distributions. Stimuli then made movements whose angle was drawn from a uniform distribution

and whose amplitude was drawn from either a normal distribution with standard deviation ranging from 20% to 100% of the diameter of the visual field or a uniform distribution of width ranging from 20% to 100% of the diameter of the visual field. 100,000 trials were simulated for each condition.

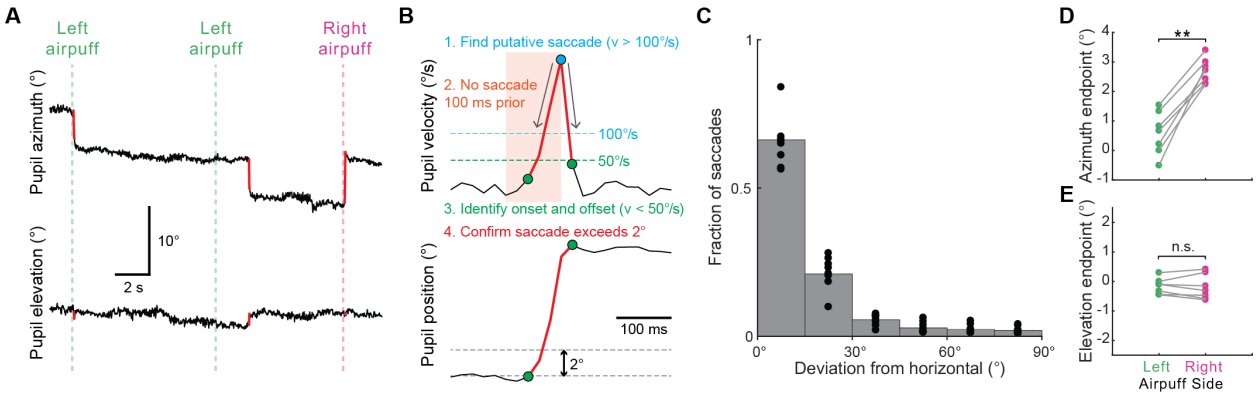

Supplementary Figure 1. Whisker airpuffs evoke horizontal saccades. **(A)** Sample traces showing pupil azimuth (top) and elevation (bottom). Segments corresponding to saccades are colored red. **(B)** Criteria for saccade detection and determination of initial and final eye positions. Top, pupil velocity is used to identify saccades and the timepoints at which the eye starts and stops moving. Red shaded area indicates 100 ms period before saccade. Bottom, pupil location is used to determine saccade amplitude and the initial position and endpoint. **(C)** Distribution of angles between airpuff-evoked saccade vectors and horizontal axis. Gray bars indicate population means and black dots indicate values for individual mice (n = 7) **(D, E)** Mean azimuth and elevation of endpoints for saccades evoked by left and right whisker airpuffs for individual mice (n = 7) (n.s., not significant; $^{**}P < 0.001$, paired two-tailed Student's t-test).

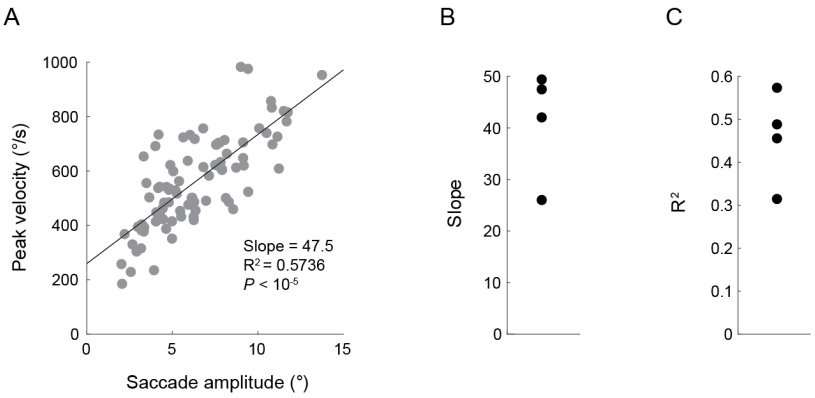

Supplementary Figure 2. WISLR saccades display a main sequence. (**A**) Peak velocity as a function of saccade amplitude for WISLR saccades for an example mouse. (**B** and **C**) Slope (B) and R^2 (C) values for individual mice (n = 4).

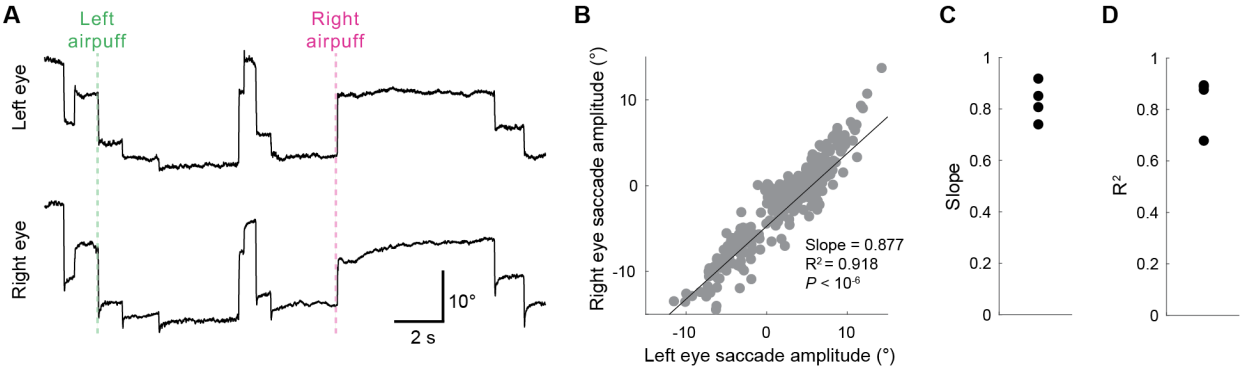

Supplementary Figure 3. WISLR saccades are conjugate. **(A)** Sample simultaneous traces of left and right eyes. **(B)** Amplitudes of left and right eye movements for each WISLR saccade made by an example animal. **(C and D)** Slope (C) and R^2 (D) values for individual mice (n = 4).

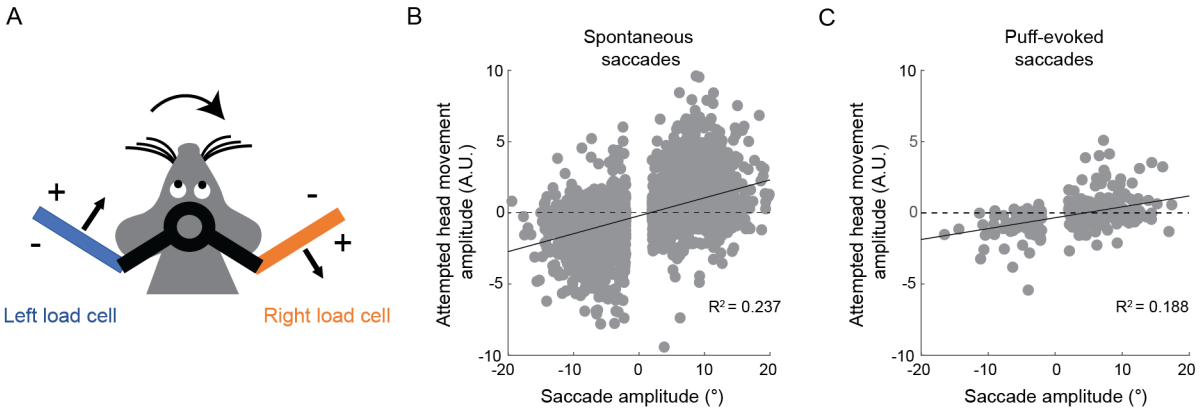

Supplementary Figure 4. WISLR saccades are associated with attempted orienting movements of the head. **(A)** Schematic of behavioral setup. Positive values correspond to attempted rightward orienting movements. **(B and C)** Relationship between spontaneous (B) and WISLR (C) saccade amplitude and attempted head movement amplitude (n = 5 mice).

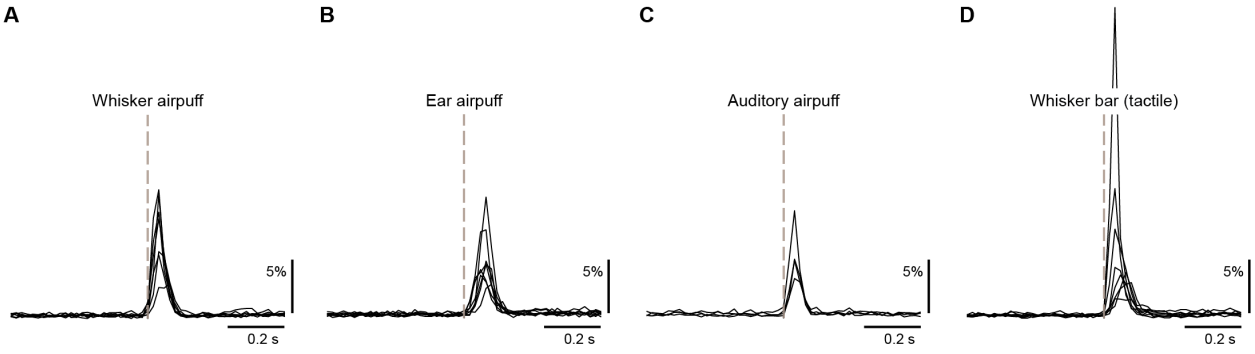

Supplementary Figure 5. Peri-stimulus time histograms showing saccade probabilities in response to whisker airpuff (A), ear airpuff (B), auditory airpuff (C), and whisker bar (D) stimulation. Each trace denotes values for a single animal.

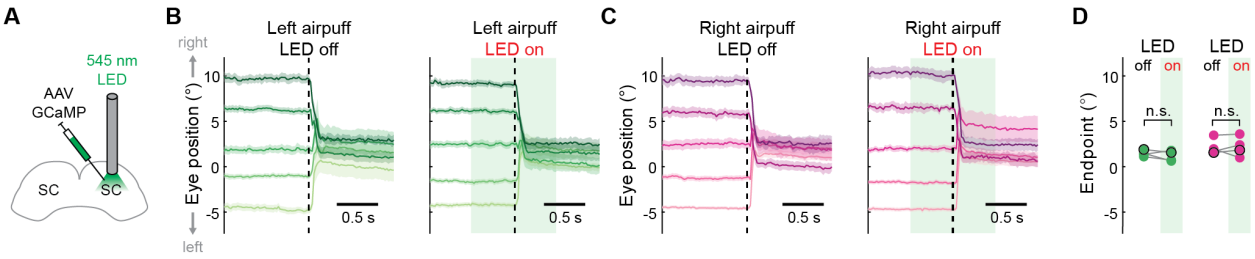

Supplementary Figure 6. Light control for optogenetic inhibition. **(A)** Schematic of fluorophore control for right SC optogenetic inhibition. **(B)** Mean saccade trajectories in response to airpuffs delivered to left whiskers on control (left) and LED on (right) trials for a representative mouse. Traces denote mean trajectories +/- s.e.m. from five different initial eye position bins. Dashed line denotes airpuff onset. Green shading denotes period of LED illumination. **(C)** As in (B) for airpuffs delivered to right whiskers. **(D)** Mean endpoints for saccades evoked by left and right whisker airpuffs on control (white background) and LED on (green background) trials for individual mice (n = 5) (n.s., not significant, paired two-tailed Student's t-test).